

MIT Open Access Articles

Chemotherapy efficiency increase via shock wave interaction with biological membranes: a molecular dynamics study

The MIT Faculty has made this article openly available. **Please share** how this access benefits you. Your story matters.

Citation: Espinosa, Silvia, Nikolaos Asproulis, and Dimitris Drikakis. "Chemotherapy Efficiency Increase via Shock Wave Interaction with Biological Membranes: a Molecular Dynamics Study." *Microfluid Nanofluid* 16, no. 4 (April 2014): 613–622.

As Published: <http://dx.doi.org/10.1007/s10404-013-1258-x>

Publisher: Springer-Verlag

Persistent URL: <http://hdl.handle.net/1721.1/87765>

Version: Author's final manuscript: final author's manuscript post peer review, without publisher's formatting or copy editing

Terms of Use: Article is made available in accordance with the publisher's policy and may be subject to US copyright law. Please refer to the publisher's site for terms of use.



Chemotherapy efficiency increase via shock wave interaction with biological membranes: a molecular dynamics study

Silvia Espinosa · Nikolaos Asproulis · Dimitris Drikakis

Received: date / Accepted: date

Abstract Application of ultrasound to biological tissues has been identified as a promising cancer treatment technique relying on temporal enhancement of biological membrane permeability via shock wave impact. In the present study the effects of ultrasonic waves on a 1,2-dipalmitoyl-sn-phosphatidylcholine (DPPC) biological membrane are examined through molecular dynamics simulations. Molecular dynamics (MD) methods traditionally employ periodic boundary conditions which, however, restrict the total simulation time to the time required for the shock wave crossing the domain, thus limiting the evaluation of the effects of shock waves on the diffusion properties of the membrane. A novel method that allows capturing both the initial shock wave transit as well as the subsequent longer-time-scale diffusion phenomena has been successfully developed, validated and verified via convergence studies. Numerical simulations have been carried out with ultrasonic impulses varying from $0.0 \text{ mPa} \cdot \text{s}$ to $0.6 \text{ mPa} \cdot \text{s}$ leading to the conclusion that for impulses $\geq 0.45 \text{ mPa} \cdot \text{s}$ no self-recovery of the bilayer is observed and, hence, ultrasound could be applied to the destruction of localized tumor cells. However, for impulses $\leq 0.3 \text{ mPa} \cdot \text{s}$ an increase of the transversal diffusivity of the lipids, indicating a consequent enhancement of drug absorption across the membrane, is initially observed followed by a progressive recovery of the initial values, thereby

suggesting the advantageous effects of ultrasound on enhancing the chemotherapy efficiency.

Keywords molecular dynamics · impulse · boundary conditions · shock wave · cancer · biological membrane

1 Introduction

Every year more than 8 million people around the globe die from cancer and more than 12 million are diagnosed for the first time, making cancer one of the leading causes of death in the western world [1]. Therefore, efforts across the scientific community have been devoted to establishing new methods as well as improving the potency and efficacy of existing ones.

The treatment of cancerous tissue with high intensity focused ultrasound (HIFU) relies on destruction of cells through conversion of mechanical energy into heat (coagulative necrosis) [2] and through mechanical damage induced by acoustic cavitation (formation and implosion of microscopic gas bubbles that generate liquid jets toward the cell membrane) [3]. The latter could be utilized not only to eliminate localized cancer tumor cells [2, 4] but also in conjunction with chemotherapy in order to temporally increase the chemotherapeutic agents absorption across the membrane [5]. The basic composition and structure of a biological membrane is often described by the fluid mosaic model [6], where the membrane is considered as a two dimensional fluid along the cell surface composed mainly of a phospholipid bilayer with embedded protein channels that allow the drug to actively penetrate into the cell. As the shock wave, following Ganzenmüller's definition [2], impacts the membrane, the lateral diffusion of the lipids and protein channels is enhanced and, hence, the prob-

S. Espinosa*

Plasma Science and Fusion Center, Massachusetts Institute of Technology, Cambridge MA 02139, USA.

S. Espinosa · N. Asproulis · D. Drikakis
Department of Engineering Physics, Cranfield University, MK43 0AL, UK.

E-mail: sesp@mit.edu, n.asproulis@cranfield.ac.uk

Table 1 Main characteristics of the topologies after solvation. A_L is the area per lipid.

System	Lipids	Atoms	Height (nm)	A_L (nm ²)
s72	72	40,020	17.51	0.6247
s128	128	73,307	17.51	0.6400
s256	256	146,227	17.51	0.6400
s72s	72	39,096	17.00	0.6247
s72b	72	41,152	18.00	0.6247

ability of the drug to be trapped by these channels is consequently increased.

By utilizing coarse graining techniques (CG), Ganzenmüller [2] concluded that, for gel phase DPPC [7], there is a critical shock wave velocity beyond which no self-recovery of the membrane is observed leading to cell disruption. The corresponding impulse (Eq. 2) was proved to be the most influential variable [8] and its critical value was estimated in the range (0.39, 0.52) $mPa \cdot s$ (Eq. 3).

Koshiyama [5] used MD to model the interaction of shock waves with biological membranes, specifically with the DPPC in crystalline phase that corresponds to the majority of body cells in nature [7], for impulses $I \in (0, 100) mPa \cdot s$. However, the use of periodic boundary conditions (PBC) restricted the total simulation time to the time required for the shock impulse to travel through the computational domain and reach the opposite side of the simulation box [5], thus leading to a large disparity between these values and the time required for studying diffusion mechanisms [7].

The aim of the present study is to investigate the response of a DPPC membrane in crystalline phase subjected to ultrasonic shocks and examine if there is a critical impulse value for which the membrane can no longer recover, in view of the ultrasound cancer treatment. In order to study long time scales of diffusion phenomena a method that allows to expand the total MD simulation time has been developed.

2 Scientific computing methods

MD employs the Newton equation of motions for each particle i

$$m_i \ddot{\mathbf{r}}_i = -\frac{\partial V_i}{\partial \mathbf{r}_i}, \quad (1)$$

where m_i is the mass of the atom i ; \mathbf{r}_i the position of the mass points; and V_i stands for the potential energy, which is a sum of semi-empirical analytical functions that model the real interatomic forces.

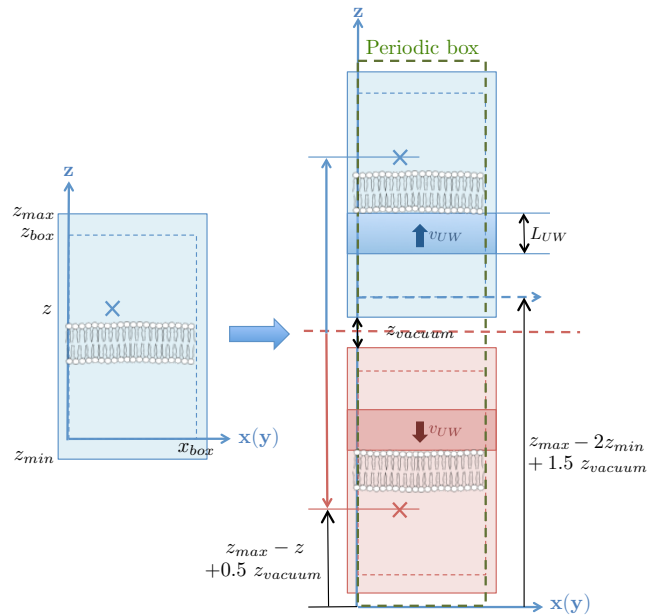


Fig. 1 Schematic of the initial configuration of shock wave simulation. The new system (right) is composed of the original system after minimization and equilibration (left) and its symmetric one. The average velocity v_{UW} is added to the thermal velocity of the water molecules in a volume $L_{UW}A$, resulting in two shock waves travelling to opposite directions away from the center of the box. The addition of a vacuum, whose size is exaggerated on the schematic, is necessary for avoiding overlapping between water molecules.

2.1 Lipid bilayer/water system

The investigation has been carried out for a DPPC membrane [7], when fixing temperature and/or pressure, at temperature 323.15 K and pressure of 1 atm [5, 9–12] corresponding to the crystalline phase [7]. The temperature coupling methods analyzed are the Berendsen [13], velocity rescaling [14] and Nosé-Hoover [15, 16] thermostats. The Berendsen algorithm mimics weak coupling with first-order kinetics to an external heat bath, suppressing the fluctuations of kinetic energy [13]. The velocity rescaling method affects the external heat flow by scaling the velocities [14]. Finally, the Nosé-Hoover thermostat extends the system Hamiltonian by introducing a friction term and a thermal reservoir in the equations of motion [15, 16]. The pressure coupling methods under study are the Berendsen [13] and Parrinello-Rahman [17] barostats. The latter allows variations not only in the volume of the domain as the former, but also in its shape.

The CHARMM 36 force field (FF) [10] and TIPS3P model [18] has been employed for lipids and water, respectively, along with the Particle Mesh Ewald (PME) [20] algorithm with cubic interpolation and no constraints, with a time step equal to 1 fs for stability purposes [18]. The CHARMM 36 FF allows the all-

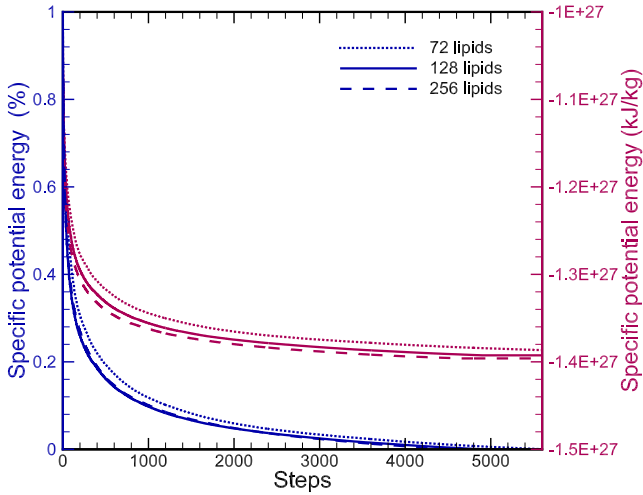


Fig. 2 Effect of the number of lipids on the specific potential energy during the energy minimization. Steepest descent algorithm with initial step size of 0.01 nm.

atom simulations of membrane and membrane-protein systems without surface tension [21] effects; the latter were found to be negligible by Tieleman [22]. The cut-off parameter for the van der Waals and Coulombic interactions is 1.0 nm [5]. The center of mass is controlled every time step separately for water and lipid molecules in order to avoid any spurious displacements of the system. Other variables, such as temperature, are also controlled separately between the lipids and the water molecules aiming to avoid any undesirable heat up of the lipids while the water is cooled down [18].

Furthermore, the leap frog integrator (LFI) is utilized for all ensembles used except for NVE, where LFI is used with the Velocity Verlet and Shift techniques for proper energy conservation [18]. Due to the high velocities arising from the application of the shock wave, the neighbor list is updated every time step instead of every 5 time steps, as in the equilibration phase. The neighbor list search cut-off distance is increased from 1.0 to 2.0 nm in the NVE simulation.

Initial topologies with 72 (named as s72 [10]), 128 and 256 (named as s128 and s256 [23]) lipids have been employed and placed parallel to the x-y plane in the centre of the periodic box. The molecular system is solvated until reaching a total height varying from 17 nm to 18 nm [5]. The main characteristics of the topologies following solvation are outlined in Table 1. According to [10], the cross section is kept squared for maintaining consistency between the numerical solution and the underlying physical phenomena.

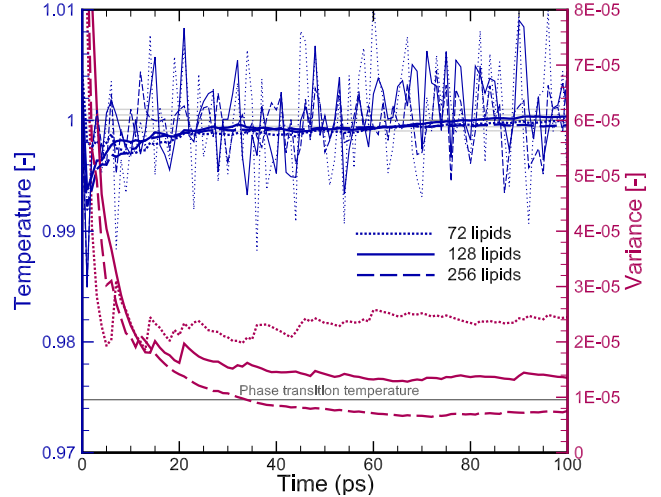


Fig. 3 Effect of the number of lipids on the temperature, its cumulative mean, represented in heavy solid line, and variance during the NVT equilibration. V-rescale temperature coupling method with period $\tau_T = 0.1ps$ and sampling period $\tau_{samp} = 1000fs$.

2.2 Shock waves modeling

The jet stream generated from the ultrasound is modeled through a rise in the momentum of the water molecules that lie within the upper layers of the simulation box that are under the effect of the ultrasonic wave. The amount of momentum transferred into the system is determined by the impulse [8]:

$$I = \int_0^{t_+} p(t)dt, \quad (2)$$

where t_+ is the positive phase duration of a half cycle of the shock wave and p is the pressure near the cells in water. Medical ultrasound has an oscillatory nature in the MHz range, and thus its characteristic time is three orders of magnitude longer than the total simulation time. Hence, an average velocity v_{UW} is added to the thermal velocity due to the ultrasonic wave:

$$v_{UW} = \frac{I \times A_{UW}}{m_{water} \cdot N_{UW}} = \frac{I \times A}{\frac{MM_{water}}{N_{av}} N_{UW}}, \quad (3)$$

where A is the transversal area of the computational box, $MM_{water} = 0.0180154 \frac{kg}{mol}$ is the molecular mass of water for the TIP3P model, N_{av} is the Avogadro number and N_{UW} number of water molecules in the water slab dictated by the thickness of the UW impact, L_{UW} . The latter is taken as 4nm as in [5], being a conservative decision since the impulses considered are one order of magnitude smaller than Koshiyama's. The ultrasound region is in contact with the zone occupied by the lipids, as in [5]. The impulses employed here are 0.3, 0.45 and 0.6 $mPa \cdot s$ corresponding to 74.92, 112.39 and 149.85 $\frac{m}{s}$, respectively.

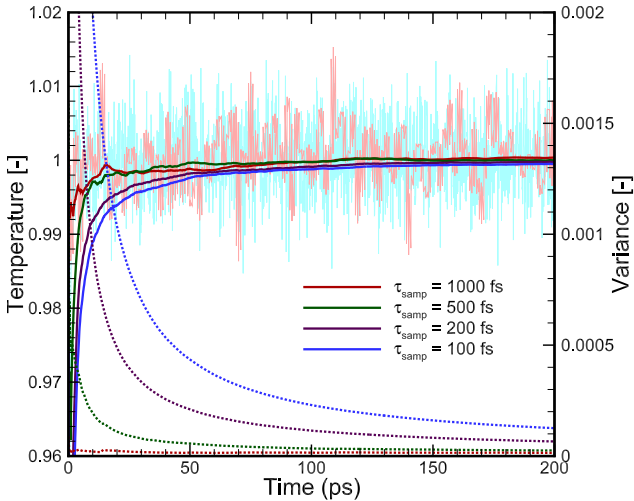


Fig. 4 Effect of sampling period on the temperature cumulative mean and variance during the NVT equilibration, represented by solid and dotted lines, respectively. The temperature is plotted for $\tau_{s\text{amp}} = 100\text{fs}$ and 1000fs . The V-rescale temperature coupling method with period $\tau_T = 0.1\text{ps}$ is used.

2.3 Boundary conditions

During minimization and equilibration, PBC with minimum image convection are employed in all three directions. During and after the shock wave impact, a new method that allows capturing both the initial shock transit as well as the subsequent longer-time-scale has been developed. The method is based on surrounding the original system by symmetric ones along the direction of the shock propagation. This is equivalent to utilizing PBC within a system composed of the original system and its symmetric one [24], as illustrated in Fig. 1. In the new system, two shock waves travel to opposite directions away from the centre of the box towards the lower and upper boundaries along the z-axis. Once the shock waves arrive at the end of the domain, due to the presence of PBC, the two waves collide and the majority of their momentum is canceled out [24].

The addition of a vacuum between the normal and the symmetric system (Fig. 1) is necessary for avoiding overlapping between water molecules. A vacuum of the same characteristics is added at the periodic boundary, so as for the method to be robust in conjunction with any MD solver. The size of the vacuum region has been selected to be of the order of a water molecule diameter (0.05 nm).

2.4 Non-dimensionalization and further analysis

The potential energy per unit of mass, pe , is given by:

$$pe = \frac{PE}{m_{\text{box}}}, \quad pe (\%) = \frac{pe - pe_{\text{final}}}{pe_{\text{initial}} - pe_{\text{final}}} \cdot 100 \quad (4)$$

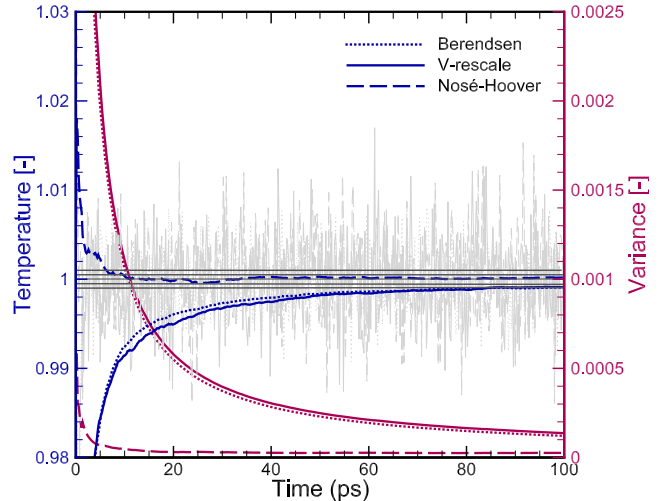


Fig. 5 Effect of the temperature coupling method on the temperature, its cumulative mean and variance, represented by grey, blue and purple lines, respectively, during the NVT equilibration. $\tau_T = 0.1\text{ps}$.

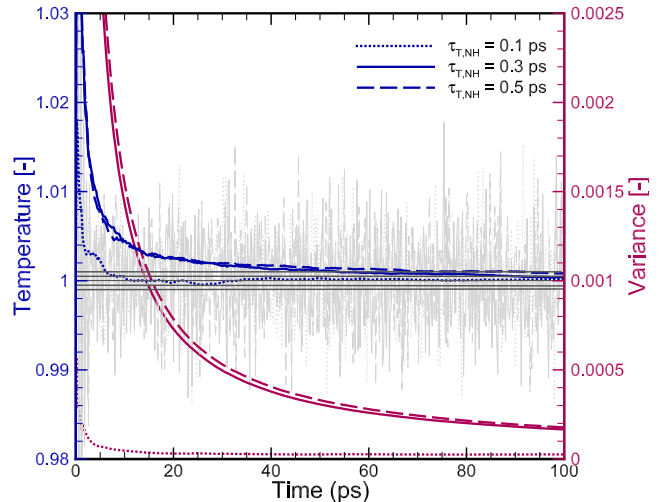


Fig. 6 Effect of the temperature coupling period on the temperature, its cumulative mean and variance, represented by grey, blue and purple respectively, during the NVT equilibration.

where PE is the potential energy and

$$m_{\text{box}} = \frac{N_L \cdot MM_L + N_W \cdot MM_W}{N_{\text{av}}} \quad (5)$$

N is the number of molecules, MW is the molecular mass and the subscripts L and W stand for lipid and water, respectively. The dimensionless temperature and pressure are obtained by dividing the dimensional values by the reference ones.

The mass and electron density profiles are calculated by dividing the periodic box in 500 slabs in the longitudinal direction and counting the particles of interest in each region [18]. The thickness of the membrane is calculated as the distance between the two

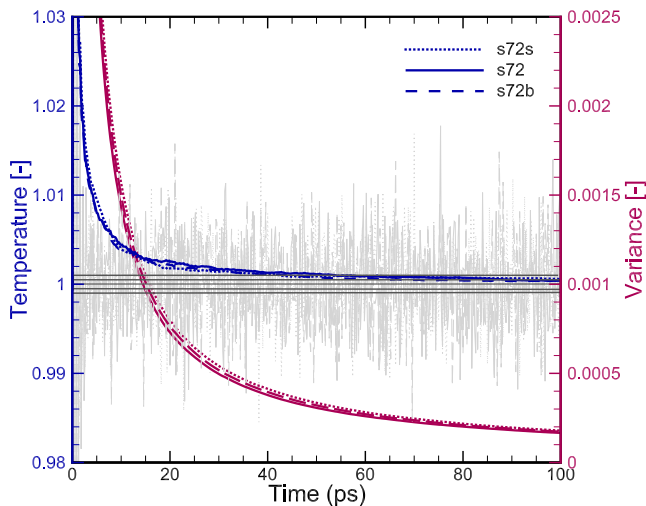


Fig. 7 Effect of the periodic box system height on the temperature, its cumulative mean and variance, represented by grey, blue and purple, respectively, during the NVT equilibration. $\tau_T = 0.3ps$.

peaks in the electron density profiles, as per experimental measurements [7]. The position of the peaks of the electron density profiles coincide with those of the phosphate electron density profiles [11], therefore when applying the shock wave the latter are utilized.

The deuterium order parameter, S_{CD} , is defined as:

$$-S_{CD} = \frac{2}{3}S_{xx} + \frac{1}{3}S_{yy}, \quad S_{ij} = \frac{1}{2}\langle 3\cos\theta_i\cos\theta_j - \delta_{ij} \rangle \quad (6)$$

where the brackets denote an ensemble average, θ_i is the angle between the i th molecular axis and the bilayer normal, and δ_{ij} is the Kronecker's delta. For the C_n methylene group, the $C_{n-1} - C_{n+1}$ direction is taken as z and the $C_{n-1} - C_n - C_{n+1}$ plane is the yz [7]. The order parameters are a measure of the spatial restriction of the motion of a CH vector. The change of length can be characterized by the averaged instantaneous deuterium order parameter [5], because the chain length becomes smaller as the disorder of chain bend angles increases.

The lateral self-diffusion coefficient of the lipids $(D_{xy})_L$ can be estimated from the slope of the averaged mean-square displacement (MSD) of the center of mass $\mathbf{x}(t)$ of single lipids by using the Einstein relation [25]:

$$\begin{aligned} (D_{xy})_L &= \frac{1}{4} \lim_{t \rightarrow \infty} \frac{1}{t} MSD \\ &= \frac{1}{4} \lim_{t \rightarrow \infty} \frac{1}{t} \langle |\mathbf{x}(t_0) - \mathbf{x}(t_0 + t)|^2 \rangle \end{aligned} \quad (7)$$

Larger slopes of the MSD implies a higher diffusion coefficient. The MSD scales proportionally to the square root of time for the single-file diffusion (SFD); linearly with time for the Fickian diffusion; and proportionally to the square of time for the ballistic diffusion characterized by a higher degree of co-ordination [26].

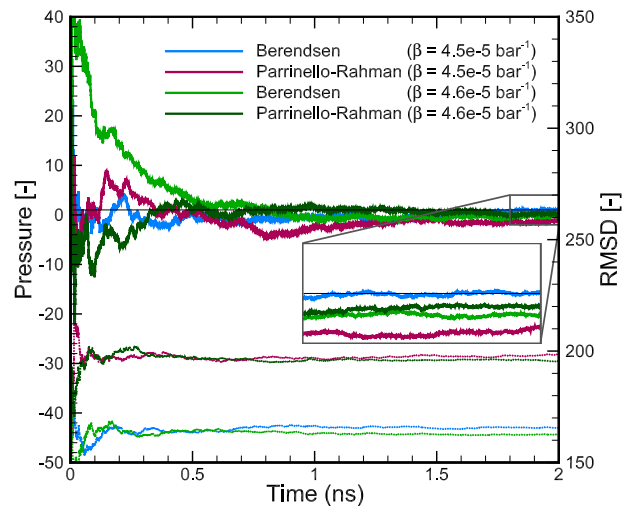


Fig. 8 Effects of the isothermal compressibility and the pressure coupling method on the cumulative mean and variance of pressure represented by solid and dotted line respectively. $\tau_T = 0.3ps$ and $\tau_P = 0.1ps$.

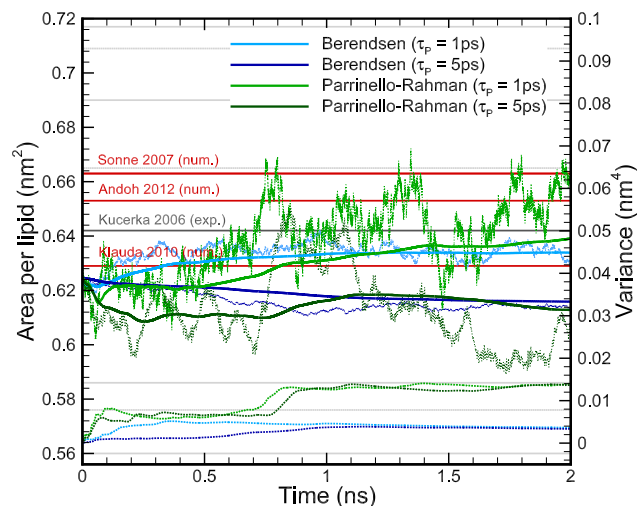


Fig. 9 Effects of the pressure coupling method and period on the area per lipid, cumulative mean and variance, represented by light dotted, thick solid and thick dotted lines, during the NPT equilibration. The validation has been carried out against experimental [9] and numerical results [10–12].

2.5 Other computational details

The double-precision GROMACS 4.5.5 [18] molecular solver has been employed in conjunction with the FTTW 3.3.2 [19] C subroutine library. The simulations have been carried out utilizing Cranfield University's HPC cluster Astral. The system uses the Intel 2012 XE Cluster Suite for compilation (FORTRAN, C, C++) and Message Passing Interface (MPI). The measured maximum performance achieved is 19.9 TFlops, though the theoretical peak processor performance is 22.5 TFlops.

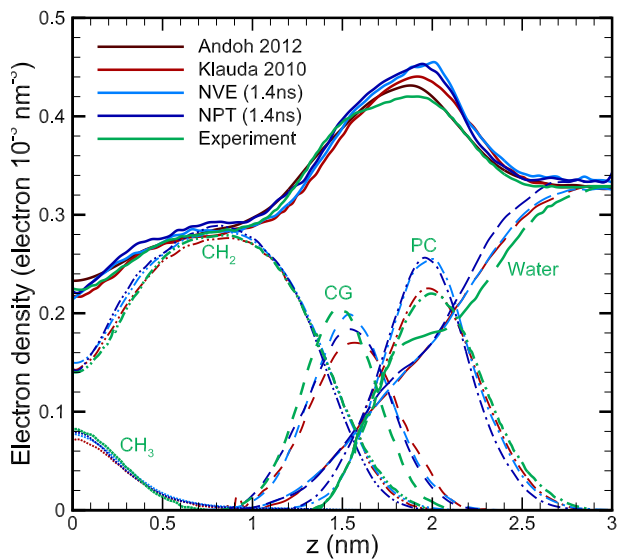


Fig. 11 Effects of the ensemble on the electron density profiles and membrane thickness. Validation has been obtained against an experimental structural model (SDP) [27] and numerical results from Klauda [10] and Andoh [11]; $z = 0$ nm corresponds to the centre of the membrane. Groups description can be found in [10].

3 Results and discussion

3.1 Minimization

Fig. 2 shows the specific potential energy during the minimization stage, for the systems s72, s128 and s256. The attractive sign demonstrates physical consistency and the potential energy values are in accordance with previously published data [18]. The results show that the higher the number of lipids is, the smaller the specific potential energy of the converged system becomes; this is due to the fact that the effect of the PBC is diminished when increasing the lipids. The differences are in any case negligible ($\Delta e < 0.7\%$).

3.2 Equilibration

In the equilibration process, consisting of a 100 ps of NVT followed by a 2 ns of NPT, different systems are simulated aiming at verifying the effects of several parameters such as number of lipids (equivalent to the parallel box size); sampling period, coupling method; characteristic coupling period; isothermal compressibility and perpendicular box size [7, 18]; and validate the results (target pressure and temperature and area per lipid) against available experimental data [9–11].

NVT stage:

In Fig. 3 the effects of the number of lipids on the temperature as a function of time are presented along with

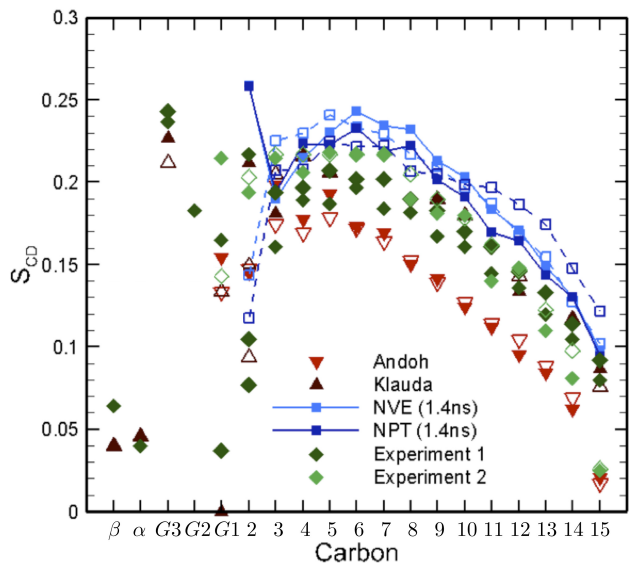


Fig. 12 Effects of the ensemble on the deuterium order parameters, S_{CD} . Validation has been obtained against nuclear magnetic resonance: experiment 1 [28–30] and experiment 2 [28, 31]; and numerical results from Klauda [10] and Andoh [11]. Open and closed symbols correspond to sn-1 and sn-2 chains, respectively.

the cumulative time average value and the corresponding variance. As the number of lipids increases the artifacts induced by the PBC diminish, thus leading to slightly decreased difference (less than 0.01%) between average and target temperature values. The associated computational cost increases by 27% for the 128 lipid case over the 72 lipids and 120% when 256 lipids are employed. Hence, it can be concluded that the 72 lipid case can sufficiently capture the dynamics of the system and provide results independent of the box size, an observation that has also been made by Klauda [10]. Therefore, for computational efficiency the s72 case is utilized for the rest of the study.

Fig. 4 shows the effect of the sampling period on the temperature mean and variance. As the sampling period decreases, movements with higher characteristic frequency occur and the root mean squared deviation (RMSD) also increases approaching that obtained when all the time steps are sampled. According to Hess [18], for lipid systems the scales of interest are captured with a sampling period $\tau_{samp} \leq 200$ fs, which is also utilized throughout the present study.

The temperature effects of the coupling method for the three approaches considered are shown in Fig. 5. For a given temperature coupling period ($\tau_T = 0.1$ ps), the Nosé-Hoover method reaches a relative error lower than 0.1%, which is more than 16 times faster compared to the other cases (Fig. 5). Moreover, even though it produces an oscillatory relaxation, the variance is smaller

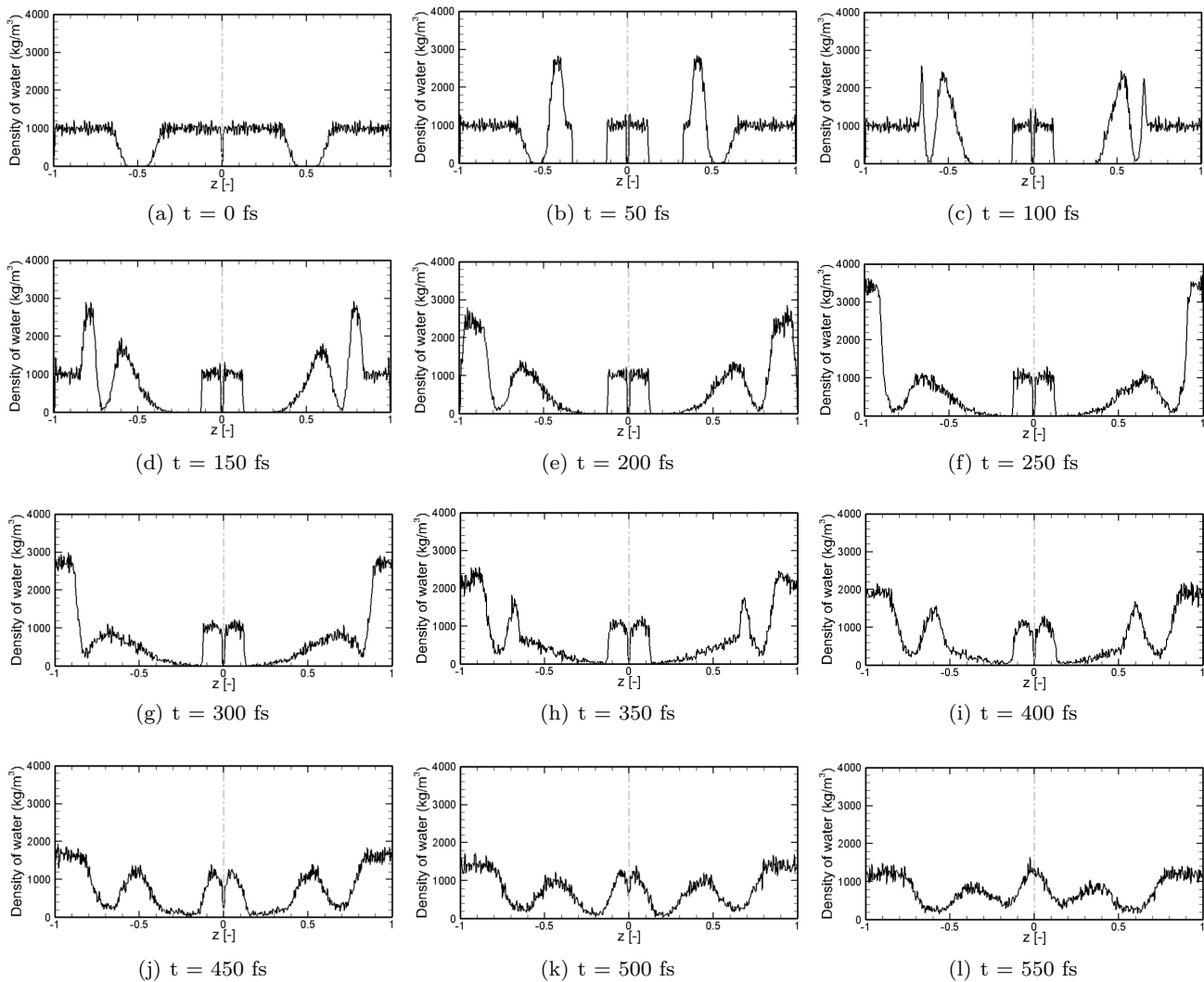


Fig. 10 Water density profiles for $I = 0.3 \text{ mPa} \cdot \text{s}$ and the NVE ensemble for time step 0.01 fs. The system is made of the original system (left) and the symmetric system (right). The hydrophobic region of the membrane in each subdomain corresponds to the region which has less than a 3% water density at $t = 0 \text{ fs}$ when compared to pure water.

than 25% compared to the ones obtained by the alternative methods. The relative error is more than two orders of magnitude smaller compared to other cases and, therefore, this is the coupling method used throughout the present study. Fig. 6 shows the effect of the temperature coupling period; it can be noticed that the relative error diminishes as the coupling period decreases until it reaches a plateau for $\tau_{T,NH} = 0.3 \text{ ps}$.

Fig. 7 shows the effect of the perpendicular box size on the temperature cumulative mean and variance. It is noticed that in the range of system height under study, 17-18nm, the effects are negligible, i.e. $\Delta e < 0.0001\%$.

NPT stage:

Fig. 8 and 9 show the effect of isothermal compressibility, pressure coupling method, and coupling period on

the values of pressure and area per lipid respectively. It is observed that the pressure coupling method does not affect significantly the relative error ($\Delta e \leq 0.5\%$), however, the RMSD obtained with Berendsen is 10% lower on average due to the fact that the exponential relation is much faster than the oscillatory one when the initial pressure value is relative far from the target one. Regarding the pressure coupling period (Fig. 9), the relative error obtained with $\tau_P = 1 \text{ ps}$ is 4 times smaller than that obtained with $\tau_P = 5 \text{ ps}$.

The pressure coupling method allows calibration via the isothermal compressibility of the membrane (Fig. 8) and the isothermal compressibility of pure water has been employed leading to minimum error for the Berendsen method and $\tau_P = 1 \text{ ps}$. This is physically consistent since the thickness of the water bilayer has

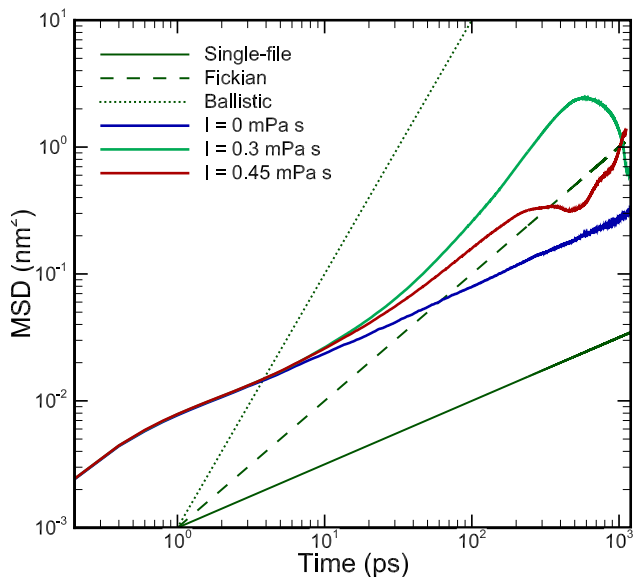


Fig. 13 Effect of the shock wave impulse on the mean squared displacement (MSD) of the lipid bilayer.

been increased so as to implement the shock wave and, hence, the system is closer to pure water than to a membrane with an embedded protein.

As a conclusion, larger sampling periods ($\tau_T = 0.3$ or 0.5 ps and $\tau_P = 5$ ps) tend to significantly overestimate pressure and result in an underestimated area per lipid, while smaller coupling periods ($\tau_T = 0.1$ ps and $\tau_P = 1$ ps) tend to slightly underestimate pressure, thus resulting in a more accurate area per lipid. The effect of the temperature coupling period is more important. When utilizing the Berendsen pressure coupling method with $\tau_{T,NH} = 0.1$ ps and $\tau_P = 1$ ps, an error lower than 1.25% is achieved, suggesting an improvement in the computational accuracy compared to the most relevant published papers [10–12] (Fig. 9).

4 Shock wave

4.1 Before the shock reaches the end of the domain

The verification of the ultrasound cancer treatment in short time scales was carried out by Koshiyama [5], who concluded that the number of lipids used in the simulation model does not significantly affect the results. Although only a qualitative comparison with Koshiyama's result is possible, due to the difference between the impulse values used in the present study and Koshiyama's, the most relevant effects associated with the collapse and rebound of bilayers and the water penetration into the hydrophobic region are observed in both studies (Fig. 10).

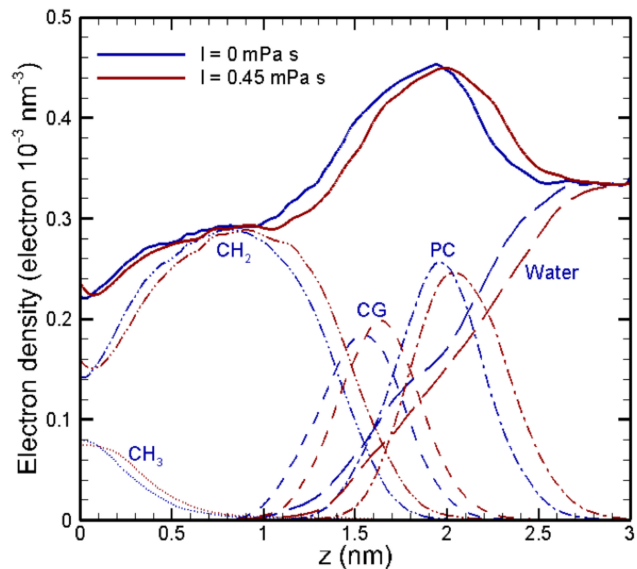


Fig. 14 Extreme increase of the thickness of the membrane at $t \approx 1.1$ ns (Fig. 13), which is a clearly evidence of the membrane desorption.

Fig. 10 shows the evolution in time of the water density profiles for $I = 0.3$ mPa · s when utilizing the NVE ensemble. The shock wave produces a high density water that induces the shrinkage of the hydrophobic region. Initially, the upper layer is pushed downwards, while the lower layer remains intact (Fig. 10b). The minimum thickness is reached when the excess of momentum is transferred to the lower layer, which is also pushed downwards (Fig. 10c). At that time, the force pushing the upper layer down becomes weaker, and the rebound stage sets in. The rebound stage is more important for water penetration than the collapse stage, as it was also observed by Koshiyama [5] (Fig. 10d-f).

When the two shock waves reach the boundary, the majority of the momentum is canceled out; following that, two shock waves of reduced intensity and speed propagate towards the axis of symmetry (Fig. 10g-l). The efficiency of the method is defined as the fraction of impulse that it is canceled out, which can be estimated as follows:

$$\begin{aligned} \text{Efficiency} &= \frac{I_1 - I_2}{I_1} \cdot 100 \\ &\approx \frac{N_{W,1}v_{s,1} - N_{W,2}v_{s,2}}{N_{W,1}v_{s,1}} \cdot 100 \approx 98\% \end{aligned} \quad (8)$$

For the present study, the efficiency of the double shocks method is around 98%, improving those of previous studies in solids [24].

4.2 After the shock reaches the end of the domain

During the NVE integration, the time step employed should be of the order of 0.01fs. Therefore, for simulating a few tens of nanosecond, 10^9 time steps are required corresponding roughly to 14 years of simulations based on the available computing resources, the size of the problem and the scalability of the solver used. According to Zhao [24], once the shock is canceled out, the simulation could be continued by using any of the commonly used ensembles. The effect of the ensemble on the results is estimated by studying the case that corresponds to $I = 0 \text{ mPa} \cdot \text{s}$, where experimental data for validation are available.

In Fig. 11 and 12, the results in the long-time scales are verified and validated in terms of electron density profile, thickness, diffusion coefficients and deuterium order parameters through comparisons with available experimental and numerical data [10, 11, 27–31]. From the analysis carried out, it is concluded that the NPT ensemble is the recommended choice due to the following reasons:

- The computational performance is ten times faster than the one obtained from the NVE ensemble.
- It is quantitatively closer to the experimental and numerical results, achieving excellent accuracy (error $< 1\%$) on the prediction of the membrane thickness, which is crucial for understanding whether or not the membrane will be disintegrated.
- As the volume is not fixed, spurious effects such as the occurrence of small densities in the centre of the box are avoided and the membrane behavior obtained corresponds to the physical one.

Finally, the effect of the impulse on the long-time scales has been investigated by selecting values closer to the critical value estimated in [2]. Following the implementation of the shock, NPT simulations with impulses 0.3 and 0.45 $\text{mPa} \cdot \text{s}$ and time steps of 1 fs and 0.5 fs respectively are carried out, increasing the pressure coupling period to 5 ps for stability.

Fig. 13 and Fig. 14 show the mean square displacement of the lipids in the membrane as function of time and the electron density profiles for different shock impulses. For impulses $\geq 0.45 \text{mPa} \cdot \text{s}$ no self-recovery of the bilayer is observed, whereas for impulses $\leq 0.3 \text{mPa} \cdot \text{s}$, the increase of the transversal diffusivity of the lipids (ballistic motion) and consequent enhancement of drug absorption across the membrane is followed by a progressive recovery of the initial values.

5 Concluding remarks

The short- and long-time scale effects of ultrasonic shock waves through DPPC lipid bilayers were investigated using MD. In respect of the long-time scale effects, a new method that utilizes symmetrical systems has been developed, validated and verified. The new method exhibits an efficiency better than other MD transmitting boundary conditions previously utilized for solids [24].

From the analysis of the long-time scales, it can be concluded that for impulses $\geq 0.45 \text{mPa} \cdot \text{s}$ no self-recovery of the bilayer is observed. However, for impulses $\leq 0.3 \text{mPa} \cdot \text{s}$, an increase of the transversal diffusivity of the lipids (ballistic motion), and consequent enhancement of drug absorption across the membrane, is noticed followed by a progressive recovery of the initial equilibrium values. Therefore, if the ultrasound method is utilized for HIFU applications, attention should be drawn to cases where $I \geq 0.45 \text{mPa} \cdot \text{s}$, whereas if the purpose of the cancer treatment is to increase the efficiency of chemotherapy, attention should focus on the range $I \leq 0.3 \text{mPa} \cdot \text{s}$. Furthermore, the research project proves numerically the efficacy of the ultrasound technique to cancer treatment.

The analysis of the response of more complex membrane models that include embedded proteins will further contribute to a better understanding of the mechanisms involved as well as optimizing the drug delivery and absorption. Furthermore, the success of the method developed has opened up the possibility of reaching time scales of medical interest that could be explored in future studies.

References

1. World Health Organization. World Health Statistics 2009. Number ISBN 97892 4 156381. World Health Organization, 2009.
2. Ganzenmüller GC, Hiermaier S, Steinhauser MO (2011) Shock-wave induced damage in lipid bilayers: a dissipative particle dynamics simulation study. *Soft Matter* 7:4307-4317. doi: 10.1039/C0SM01296C
3. Vogel A, Busch S, Parlitz U (1996) Shock wave emission and cavitation bubble generation by picosecond and nanosecond optical breakdown in water. *J Acoust Soc Am* 100(1):148-165. doi:10.1121/1.415878
4. Brú A, Casero D (2006) The effect of pressure on the growth of tumour cell colonies. *J Theor Biol* 243:171-180. doi:10.1016/j.jtbi.2006.05.020
5. Koshiyama K, Kodama T, Yano T, Fijikawa S (2006) Structural change in lipid bilayers and water penetration induced by shock waves: molecular dynamics simulations. *Biophys J* 91(6):2198-2205. doi: 10.1529/biophysj.105.077677
6. Singer SJ, Nicholson GL (1972) The fluid mosaic model of the structure of cell membranes. *Science* 175(4023):720-731. doi:10.1126/science.175.4023.720

7. Tieleman DP, Marrink SJ, Berendsen HJC (1997) A computer perspective of membranes: molecular dynamics studies of lipid bilayer systems. *Biochim Biophys Acta* 1331:235-270. doi:10.1016/S0304-4157(97)00008-7
8. Kodama T, Hamblin MR, Doukas AG (2000) Cytoplasmic molecular delivery with shock waves: importance of impulse. *Biophys J* 79:1821-1832. doi: 10.1016/S0006-3495(00)76432-0
9. Kucerka N, Tristram-Nagle S, Nagle JF (2006) Closer look at structure of fully hydrated fully hydrated fluid phase DPPC bilayers. *Biophys J* 90(11): L83L85. doi: 10.1529/biophysj.106.086017
10. Klauda JB, Venable RM, Freites JA, Connor JW, Tobias DJ, Mondragon-Ramirez C, Vorobyov I, MacKerell AD, Pastor RW (2010) Update of the CHARMM all-atom additive force field for lipids: validation on six lipid types. *J Phys Chem B* 114(23):78307843. doi: 10.1021/jp101759q
11. Andoh Y, Ito T, Okazaki S (2012) An application of improved force field to fully hydrated DPPC and POPC bilayers in a tensionless NPT ensemble: a test of CHARMM 27-based new force field by Högberg et al. *Molecular simulation* 38(5):414418. doi: 10.1080/08927022.2010.548385
12. Sonne J, Jensen MO, Hansen FY, Hemmingsen L, Peter GH (2007) Reparametrization of all-atom dipalmitoylphosphatidylcholine lipid parameters enables simulation. *Biophys J* 92(12):4157-4167. doi: 10.1529/biophysj.106.087130
13. Berendsen HJC, Postma JPM, van Gunsteren WF, Dinola A, Haak JR (1984) Molecular dynamics with coupling to an external bath. *J Chem Phys* 81(8):3684-3690. doi:10.1063/1.448118
14. Bussi G, Donadio D, Parrinello M (2007) Canonical sampling through velocity rescaling. *J Chem Phys* 126(1):014-101. doi:10.1063/1.2408420
15. Nosé S (1984) A molecular dynamics method for simulations in the canonical ensemble. *Mol Phys* 31(3):1695-1697. doi:10.1080/00268978400101201
16. Hoover WG (1985) Canonical dynamics: Equilibrium phase-space distributions. *Phys Rev A* 31(3):1695-1697. doi:10.1103/PhysRevA.31.1695
17. Parrinello M, Rahman A (1981) Polymorphic transitions in single crystals: A new molecular dynamics method. *J Appl Phys* 52(12):7182-7190. doi:10.1063/1.328693
18. Hess B, Kutzner C, Spoel D, Lindahl E (2008) GRO-MACS 4: Algorithms for highly efficient, load-balanced, and scalable molecular simulation. *J Chem Theory Comput* 4(3):435-447. doi: 10.1021/ct700301q
19. Frigo M and Johnson SG (2005) The design and implementation of FFTW3. *Proceedings of the IEEE*, 93(2):216-231. doi:10.1109/JPROC.2004.840301
20. Ewald PP (1921) Die Berechnung optischer und elektrostatischer Gitterpotentiale. *Ann Phys* 369(3): 253-287.
21. Freites JA, OConnor JW, Tobias DJ, Mondragon-Ramirez C, Vorobyov I, MacKerell AD, Klauda JB, Venable RM and Pastor JW (2010) Update of the CHARMM all-atom additive force field for lipids: Validation on six lipid types. *J Chem Phys B*, 114:7830-7843.
22. Tieleman DP, Berendsen HJC. (1996) Molecular dynamics simulations of a fully hydrated dipalmitoylphosphatidylcholine bilayer with different macroscopic boundary conditions and parameters. *J Chem Phys* 105(11):4871-4880. doi:10.1063/1.472323
23. Jo S, Kim T, Im W (2007) Automated builder and database of protein/membrane complexes for molecular dynamics simulations. *PLoS ONE* 2(9):e880. doi:10.1371/journal.pone.0000880
24. Zhao S, Germann TC, Strachan A (2006) Atomistic simulations of shock-induced alloying reactions in Ni/Al nanolaminates. *J Chem Phys* 125(16):164707-164714. doi:10.1063/1.2359438
25. Bockmann RA, Hac A, Heimburg T, Grubmüller H (2003) Effect of sodium chloride on a lipid bilayer. *Biophys J* 85(3):1647-1655. doi:10.1016/S0006-3495(03)74594-9
26. Striolo A (2006) The mechanism of water diffusion in narrow carbon nanotubes. *Nano Lett*, 6(4):633639. doi:10.1021/nl052254u
27. Kucerka N, Nagle JF, Sachs JN, Feller SE, Pencer J, Jackson A, Katsaras J (2008) Lipid bilayer structure determined by the simultaneous analysis of neutron and X-ray scattering data. *Biophys J* 95(5):2356-2367. doi:10.1529/biophysj.108.132662
28. Seelig A, Seelig J (1975) Bilayers of dipalmitoyl-3-sn-phosphatidylcholine. Conformational differences between the fatty acyl chains. *Biochim Biophys Acta*, 406(1). doi:10.1016/0005-2736(75)90037-1
29. Seelig A, Seelig J (1974) Dynamic structure of fatty acyl chains in a phospholipid bilayer measured by deuterium magnetic resonance. *Biochemistry* 13(23):4839-4845. doi:10.1021/bi00720a024
30. Klauda JB, Eldho NV, Gawrisch K, Brooks BR, Pastor RW (2008) Collective and noncollective models of NMR relaxation in lipid vesicles and multilayers. *J Phys Chem J* 112(19):5924-5929. doi:10.1021/jp075641w
31. Douliez JP, Leonard A, Dufourc EJ (1995) Restatement of order parameters in biomembranes - calculation of C-C bond order parameters from C-D quadrupolar splittings. *Biophys J* 68(5):1727-1739.